# A New Method for Estimation of the Sensible Heat Flux under Unstable Conditions Using Satellite Vector Winds

JIAYI PAN,* XIAO-HAI YAN, YOUNG-HEON JO, AND QUANAN ZHENG

*Graduate College of Marine Studies, University of Delaware, Newark, Delaware*

W. TIMOTHY LIU

*Jet Propulsion Laboratory, California Institute of Technology, Pasadena, California*

18 February 2003 and 21 August 2003

ABSTRACT

It has been difficult to estimate the sensible heat flux at the air–sea interface using satellite data because of the difficulty in remotely observing the sea level air temperature. In this study, a new method is developed for estimating the sensible heat flux using satellite observations under unstable conditions. The basic idea of the method is that the air–sea temperature difference is related to the atmospheric convergence. Employed data include the wind convergence, sea level humidity, and sea surface temperature. These parameters can be derived from the satellite wind vectors, Special Sensor Microwave Imager (SSM/I) precipitable water, and Advanced Very High Resolution Radiometer (AVHRR) observations, respectively. The authors selected a region east of Japan as the test area where the atmospheric convergence appears all year. Comparison between the heat fluxes derived from the satellite data and from the National Centers for Environmental Prediction (NCEP) data suggests that the rms difference between the two kinds of sensible heat fluxes has low values in the sea area east of Japan with a minimum of 10.0 W $m^{-2}$. The time series of the two kinds of sensible heat fluxes at 10 locations in the area are in agreement, with rms difference ranging between 10.0 and 14.1 W $m^{-2}$ and correlation coefficient being higher than 0.7. In addition, the National Aeronautics and Space Administration (NASA) Goddard Satellite-Based Surface Turbulent Flux (GSSTF) was used for a further comparison. The low-rms region with high correlation coefficient ($>0.7$) was also found in the region east of Japan with a minimum of 12.2 W $m^{-2}$. Considering the nonlinearity in calculation of the sensible monthly means, the authors believe that the comparison with GSSTF is consistent with that with NCEP data.

## 1. Introduction

The sensible heat flux in the ocean surface plays an important role in the energy balance between the ocean and atmosphere. The sensible heat flux is a direct physical contact of the atmosphere and ocean and it enables energy to be exchanged between them by conduction (Bigg 1996). Through sensible heat flux, the oceans absorb (release) the heat energy from (to) the atmosphere, compensating the temperature sharp change in the atmosphere and adjusting the local climate and beyond.

Conventionally, the sensible heat flux can be calculated using the bulk formula,

$$Q_s = \rho C_H C_p (T_w - T_a) U, \quad (1)$$

where $\rho$ is the atmospheric density, $C_H$ is the transfer coefficients for sensible heat flux, $C_p$ is the specific heat of air, and $T_w$ and $T_a$ are the sea surface temperature and air temperature, respectively. A typical range of $C_H$ is from $1.1 \times 10^{-3}$ in an atmosphere with much vertical mixing to $0.8 \times 10^{-3}$ in stratified air. Using the bulk formula and satellite observations to estimate the sensible heat flux, we need to know the sea surface and air temperatures. The sea surface temperature can be retrieved from observations with the Advanced Very High Resolution Radiometers (AVHRR) on the National Oceanic and Atmospheric Administration (NOAA) satellites. However, it is difficult to remotely observe the sea level air temperature. We have to resort to in situ measurements of the air temperature. It is expensive and time-consuming to make direct measurements on large

* Current affiliation: Department of Marine Science, University of Southern Mississippi, Stennis Space Center, Mississippi.

*Corresponding author address:* Dr. Jiayi Pan, Department of Marine Science, University of Southern Mississippi, 1020 Balch Blvd., Stennis Space Center, MS 39529.
E-mail: jiayi.pan@usm.edu

scale. Therefore, numerical model methods were used to calculate the sensible heat flux on the basis of simulated air temperature. Bagno and Zalesny (1992) used a primitive ocean dynamics model to simulate the annual cycle of hydrological fields for the North Atlantic region, and the model generated sensible, latent, and solar radiation heat fluxes on the basis of a simplified parameterization. Cai and Godfrey (1995) described a series of experiments using the Geophysical Fluid Dynamics Laboratory (GFDL) modular ocean model for the Atlantic Ocean forced by a fixed freshwater flux and two different heat flux parameterization schemes. Giese and Cayan (1993) used models of the tropical Pacific Ocean and bulk formulae to estimate the sea surface fluxes of the heat into and out of the ocean. He et al. (1997) developed a one-dimensional, level-2.5 turbulence closure inverse mixed layer model and calculated the surface heat fluxes in the western equatorial Pacific using the bulk parameterization. Their results showed that the numerical model generates large variations in daily mean heat flux estimates while the derived longer time-averaged net heat flux is more consistent with the bulk formula result. Baumgartner and Anderson (1999) evaluated flux fields provided by three of the regional numerical weather prediction (NWP) models in operation during 1996 and 1997 at the U.S. National Centers for Environmental Prediction (NCEP): the Eta-48, Eta-29, and Rapid Update Cycle (RUC-1) models. These model fields were compared with in situ measurements made from an air–sea interaction buoy depolyed from July 1996 to June 1997 at a midshelf location in the Middle Atlantic Bight during the Coastal Mixing and Optics Experiment. In light of these evaluations, considerations for improving the accuracy of the surface flux fields for use in future ocean modeling studies were suggested.

Recently, satellite observations have become an increasingly accurate and reliable data source for ocean and atmosphere studies. Efforts to estimate the sensible heat flux using satellite data have been undertaken for many years. A local relationship between near-surface air temperature and precipitation was developed by Thadathil et al. (1993) for the sensible heat flux calculation. Using Special Sensor Microwave Imager (SSM/I) data and a bulk aerodynamic parameterization method, Simon et al. (1998) estimated near-surface specific humidity, sea surface temperature (SST), and near-surface air temperature. The sensible and latent heat fluxes were calculated from these parameters. The evaporation estimate as based on these satellite parameters was also assessed by comparison with ship observations. Konda et al. (1996) derived an equation relating the near-sea air temperature with other parameters in the boundary layer that can be observed by satellite sensors.

In this study, we introduce a new method to estimate the sea surface air temperature under unstable conditions based on the scatterometer winds for calculation of the sensible heat flux using the bulk formula. The next section gives a description of the new method. Section 3 depicts satellite data used in the calculation. The comparison and result are given in section 4. Section 5 is discussions and conclusions of this study.

## 2. The methodology description

When the sea surface temperature is higher than the air temperature, atmospheric convergence can take place. This phenomenon was observed by Pan et al. (2002). Assuming that the air over the sea surface is an ideal gas, we have state equations for the air above and at the sea surface as

$$p = \rho_a T_a R_d (1 + 0.608q) \quad \text{and} \tag{2}$$

$$p = \rho_w T_w R_d (1 + 0.608Q), \tag{3}$$

where $p$ is the pressure; $\rho$ is the air density; the subscripts $a$ and $w$ represent the situation above and at the sea surface, respectively; $Q$ and $q$ are the specific humidity, and stand for the saturated specific humidity at the temperature $T_w$ and the humidity in the air at the temperature $T_a$; and $R_d$ is the dry air constant. We know that

$$Q = 0.622\frac{e}{p} \quad \text{and} \tag{4}$$

$$e = E_0 \times 10^{aT_w^c/(b+T_w^c)}, \tag{5}$$

where $e$ is the saturated vapor pressure, $E_0 = 6.11$ hPa, $a = 7.5$, $b = 237.3$, and $T_w^c$ represents the water temperature (°C). The mixing ratio $m$ is given by an empirical formula developed by Liu (1986):

$$m = 3.818\,724W + 0.189\,721\,9W^2 + 0.189\,189\,3W^3 - 0.075\,490\,36W^4 + 0.006\,088\,244W^5, \tag{6}$$

where $W$ represents the precipitable water and can be observed by the satellite sensor SSM/I. Because dry air is heavier than the water vapor in a certain volume of air, the mix ratio equals approximately the specific humidity $q$.

The buoyancy force $F$ acting on a unit mass of air is

$$F = \frac{\rho_a - \rho_w}{\rho} g = \frac{\Delta\rho}{\rho} g \tag{7}$$

and can be written as

$$F = \frac{\Delta\rho}{\rho} g = \frac{dw}{dt}. \tag{8}$$

We assume that the air density change is small and the following continuity equation is still effective:

$$\frac{dw}{dz} = -\left(\frac{du}{dx} + \frac{dv}{dy}\right), \tag{9}$$

where $u$ and $v$ represent horizontal velocity, and $w$ stands for vertical velocity. Defining the atmospheric convergence as $C = -(du/dx + dv/dy)$, we can relate $C$ with $\Delta\rho$ by

$$\frac{\Delta\rho}{\rho}g = \frac{dw}{dt} = \frac{dw}{dz}\frac{dz}{dt} = C\frac{dz}{dt}, \quad \text{or} \tag{10}$$

$$\Delta\rho = \frac{C\rho}{g}\frac{dz}{dt}. \tag{11}$$

Based on (2) and (3), $\Delta\rho$ can be derived as

$$\begin{aligned}\Delta\rho &= \frac{p}{T_a R_d(1 + 0.608q)} - \frac{p}{T_w R_d(1 + 0.608Q)} \\ &= \frac{p(T_w - T_a)}{T_w T_a R_d(1 + 0.608q)} \\ &\quad + \frac{0.608(Q - q)p}{T_w R_d(1 + 0.608q)(1 + 0.608Q)} \\ &= \frac{p(T_w - T_a)}{T_w[T_w - (T_w - T_a)]R_d(1 + 0.608q)} \\ &\quad + \frac{0.608(Q - q)p}{T_w R_d(1 + 0.608q)(1 + 0.608Q)}. \end{aligned} \tag{12}$$

Let $\Delta T = T_w - T_a$ and, because kelvin temperatures are used in (12), we have $\Delta T/T_w \ll 1$; (12) can be further written as

$$\begin{aligned}\Delta\rho &= \frac{p\Delta T}{T_w^2\left(1 - \frac{\Delta T}{T_w}\right)R_d(1 + 0.608q)} \\ &\quad + \frac{0.608(Q - q)p}{T_w R_d(1 + 0.608q)(1 + 0.608Q)} \\ &= \frac{p\Delta T}{T_w^2 R_d(1 + 0.608q)}\left(1 + \frac{\Delta T}{T_w}\right) \\ &\quad + \frac{0.608(Q - q)p}{T_w R_d(1 + 0.608q)(1 + 0.608Q)} + O\left[\left(\frac{\Delta T}{T_w}\right)^2\right] \\ &= \frac{p\Delta T}{T_w^2 R_d(1 + 0.608q)} \\ &\quad + \frac{0.608(Q - q)p}{T_w R_d(1 + 0.608q)(1 + 0.608Q)} \\ &\quad + \frac{p}{T_w R_d(1 + 0.608q)}\left(\frac{\Delta T}{T_w}\right)^2 + O\left[\left(\frac{\Delta T}{T_w}\right)^2\right] \\ &= \frac{p\Delta T}{T_w^2 R_d(1 + 0.608q)} \\ &\quad + \frac{0.608(Q - q)p}{T_w R_d(1 + 0.608q)(1 + 0.608Q)} + O\left[\left(\frac{\Delta T}{T_w}\right)^2\right]. \end{aligned} \tag{13}$$

In (13), neglecting the second order term $O(\Delta T/T)^2$, we have

$$\begin{aligned}\Delta\rho &\approx \frac{p\Delta T}{T_w^2 R_d(1 + 0.608q)} \\ &\quad + \frac{0.608(Q - q)p}{T_w R_d(1 + 0.608q)(1 + 0.608Q)}. \end{aligned} \tag{14}$$

Therefore, the air–sea temperature difference is derived as

$$\Delta T = \frac{\Delta\rho T_w^2 R_d(1 + 0.608q)}{p} - \frac{0.608(Q - q)T_w}{1 + 0.608Q}. \tag{15}$$

Substituting $\Delta\rho$ with (11), $\Delta T$ can be written as

$$\Delta T = \frac{dz}{dt}\frac{\rho_a C T_w^2 R_d(1 + 0.608q)}{gp} - \frac{0.608(Q - q)T_w}{1 + 0.608Q}. \tag{16}$$

Let $dz/dt = K$ and combine it with (1); then we have a new sensible heat calculation formula as

$$Q_s = \rho_a C_H C_P U\left[\frac{K\rho_a C T_w^2 R_d(1 + 0.608q)}{gp} - \frac{0.608(Q - q)T_w}{1 + 0.608Q}\right]. \tag{17}$$

On the basis of (17), we constructed a relationship between sensible heat flux and atmosphere convergence. The sensible heat flux can be calculated using a series of satellite observations.

## 3. Satellite data

Equation (17) relates the sensible heat flux with the atmosphere convergence ($C$), sea surface temperature ($T_w$), and specific humidity. These parameters can be obtained from the satellite observations, which implies that we can estimate the sensible heat flux completely using the satellite data. The satellite data are described as follows.

### *a. Scatterometer vector winds and atmospheric convergence*

We used *European Remote Sensing Satellite* (*ERS*)*-1/2* scatterometer vector winds for deriving the atmospheric convergence. *ERS-1* was launched in July 1991. The Active Microwave Instrument (AMI) on board *ERS-1* could act as a C-band (5.3 GHz) scatterometer, which measured backscattering of the ocean surface and retrieved both wind speed and wind direction. *ERS-2*, the successor to *ERS-1*, was launched in April 1995, and carried the same instruments as *ERS-1*. *ERS-1/2* scatterometer measurements were processed in the Centre ERS d'Archivage et de Traitement (CERSAT) of the French Research Institute for Exploitation of the Sea (IFREMER) for generating the wind products. The $1° \times 1°$ gridded wind products consist of weekly and monthly wind fields, covering the period beginning on 5 August 1991. In this study, *ERS-1/2* scat-

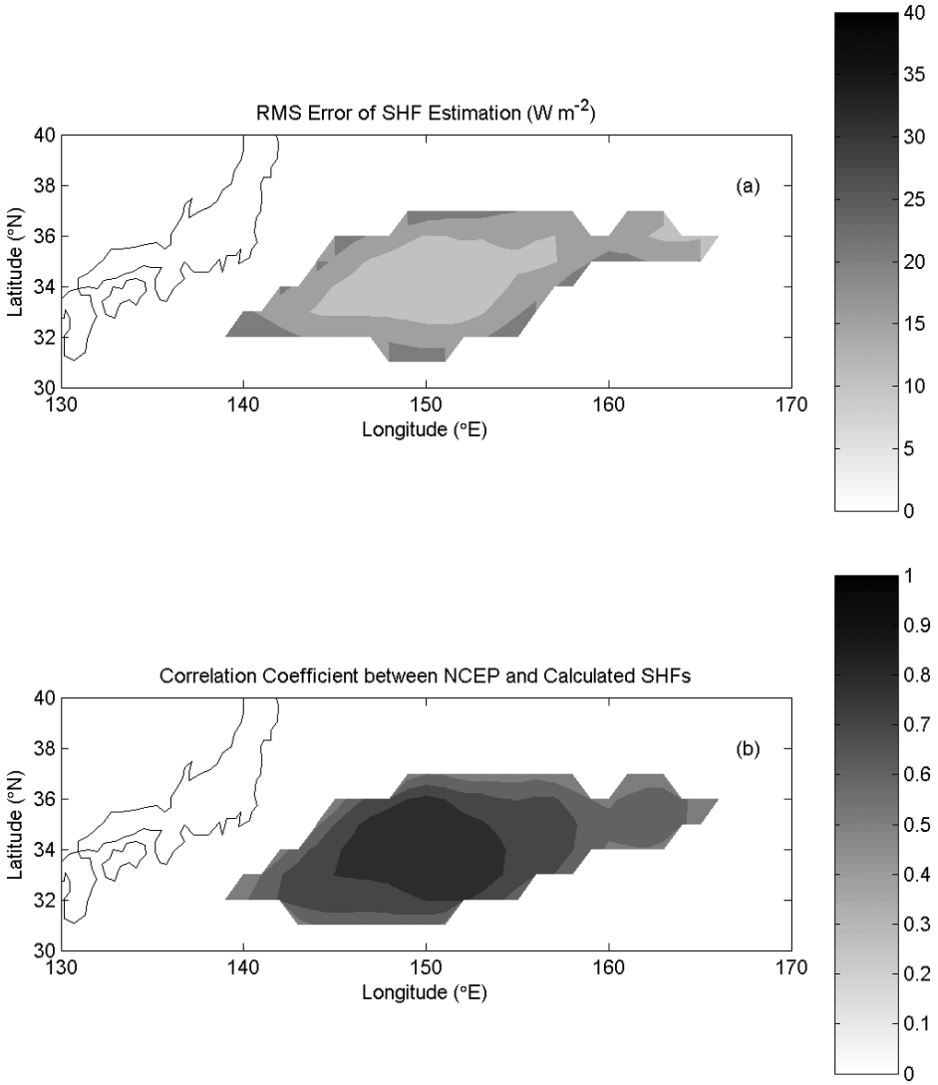


FIG. 1. (a) Rms difference and (b) correlation coefficient between the sensible heat flux calculated from satellite data and that derived from NCEP air temperature.

terometer winds from July 1993 to December 1998 were used. These datasets and description documenters are available online at http://www.ifremer.fr/cersat/en/data/download/download.htm.

The discrete form of the convergence is given as

$$C_{i,j} = -\left(\frac{u_{i+1,j} - u_{i,j}}{\Delta x} + \frac{v_{i,j+1} - v_{i,j}}{\Delta y}\right). \qquad (18)$$

For the $1^\circ \times 1^\circ$ grid, $\Delta x$ and $\Delta y$ are written as follows:

$$\Delta x = \frac{\pi R}{180}\cos\theta \quad \text{and} \quad \Delta y = \frac{\pi R}{180}, \qquad (19)$$

where $R$ is the radius of the earth and $\theta$ is the latitude. When $C$ is greater than zero, atmospheric convergence takes place, and a strong atmospheric convergence zone appears with large positive $C$ (Zheng et al. 1997; Pan et al. 2002).

### *b. SSM/I scalar winds and precipitable water*

The wind speed in (1) is a scalar, which requires a scalar average for calculation of the monthly sensible heat flux. The scatterometer vector winds cannot sever for this purpose. We chose a scalar wind product (SSM/I) wind speed dataset. The SSM/I only observes wind speed regardless of direction. Therefore, the means of the wind product are the scalar averages of the wind speed. The Defense Meteorological Satellite Program (DMSP) Special Sensor Microwave Imager became operational in July 1987 and was a seven-channel passive microwave radiometer operating at four frequencies (19.35, 22.235, 37.0, and 85.5 GHz) and dual polarization (except at 22.235 GHz, which is V-polarization only). The SSM/I provided products such as rainfall rate, rainfall frequency, cloud liquid water, cloudiness frequency, total precipitable water, snow cover, sea ice,

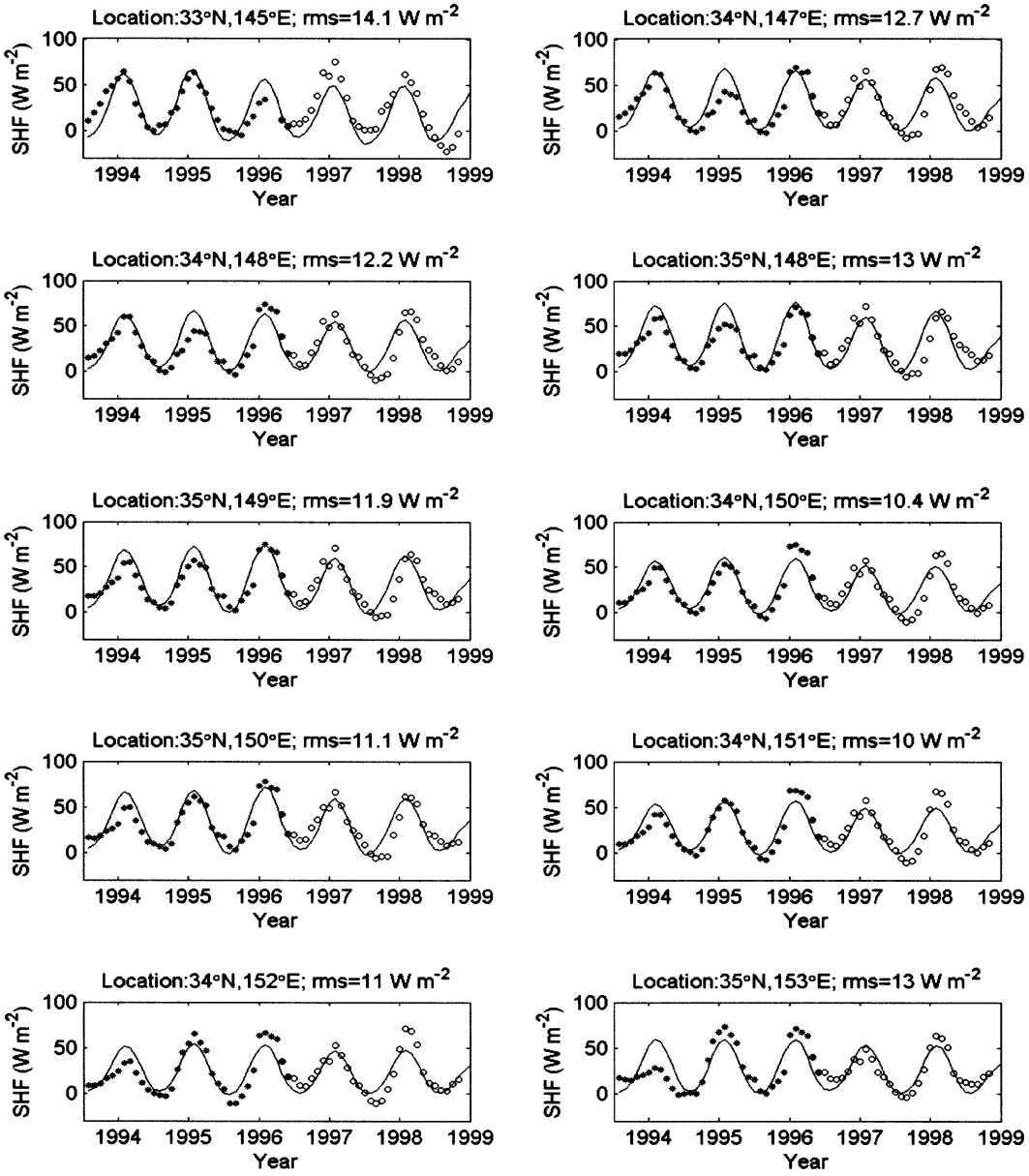


FIG. 2. The time series of satellite-data-calculated sensible heat flux (*: *ERS-1*, ○:*ERS-2*) and NCEP-air-temperature-derived flux (solid line) at 10 locations in the test area from Jul 1993 to Dec 1998.

sampling frequency, and ocean surface wind speed. These products are useful for evaluating the mean climate state and its interannual and seasonal variations (Liu et al. 1992). We used the monthly mean wind speed dataset, which has the $1° \times 1°$ grid and covers the period from July 1993 to December 1998.

The SSM/I precipitable water data were used for calculation of the humidity, based on an empirical relationship [Eq. (6)]. Like the wind speed dataset, the humidity is monthly on a $1° \times 1°$ grid, covering the period from July 1993 to December 1998. Detailed descriptions of the datasets can be found online at the Remote Sensing System Web site: http://www.ssmi.com/ssmi/ssmi_description.html#ssmi.

### c. Sea surface temperature

The sea surface temperature (SST) data are the Pathfinder Best-SST data product. This product consists of daily and monthly SST data derived from the five-channel AVHRRs on board the *NOAA-7*, *-9*, *-11*, and *-14* polar-orbiting satellites. Unlike the AVHRR Pathfinder All-SST product, only the highest-quality pixel values are retained in this product. For this study, we used the

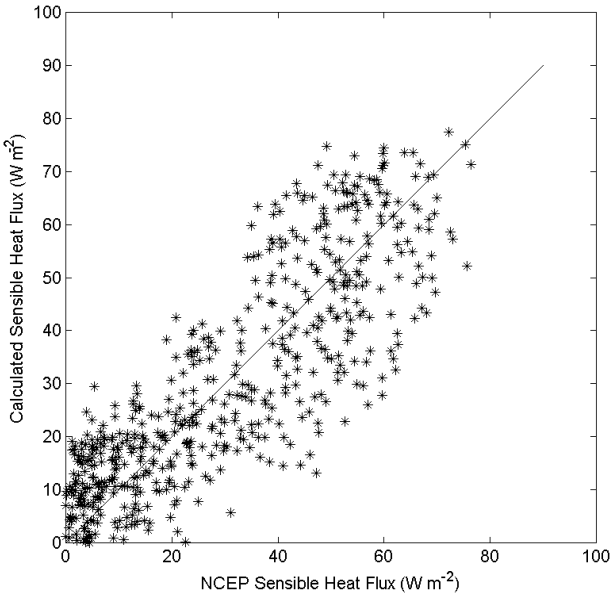


FIG. 3. Scatterplot of the satellite-data-calculated sensible heat flux and NCEP-air-temperature-derived flux at 10 locations in the test area.

monthly dataset with the spatial grid of $1° \times 1°$ (Vazquez et al. 1996).

## 4. Comparison and results

### a. Climatological analysis

The atmospheric convergence $C$ was calculated from scatterometer winds for the period from July 1993 to December 1998. In order to calculate the sensible heat flux on the basis of (17), we need to know $K$, which varies from place to place. In this study, we determine $K$ by employing the clamotological sea surface air temperature and satellite data. The climatological air temperature is from the Comprehensive Ocean–Atmosphere Data Set (COADS), provided by the NOAA–CIRES Climate Diagnostics Center's Web site, found online at http://www.cdc.noaa.gov/. First, using the climatological sea surface air and water temperature, we calculated the climatological sensible heat flux, which is represented as $\mathrm{SHF}_c$. Then, we derived climatological monthly means of wind convergence, sea surface temperature, and humidity from satellite data and calculated the right-hand-side terms of (17),

$$\rho_a C_H C_P U \frac{\rho_a C T_w^2 R_d (1 + 0.608q)}{gp} \quad \text{and}$$

$$-\rho_a C_H C_P U \frac{0.608(Q - q)T_w}{1 + 0.608Q};$$

the two terms are represented as $A$ and $B$, respectively. Some constants are $\rho = 1.293$ (kg m$^{-3}$); $p = 1013.25$ (hPa); $R_d = 287.05$ (J kg$^{-1}$ K$^{-1}$); $C_p = 1.006 \times 10^3$ (J kg$^{-1}$ °C$^{-1}$); and $C_H = 1.13 \times 10^{-3}$, which is the bulk coefficient under unstable conditions (Large and Pond 1982). Large and Pond's result revealed that the standard deviation of $C_H$ is close to $0.14 \times 10^{-3}$ in a very unstable situation. This result implies that in this study, the uncertainty of $C_H$ caused about 12% errors.

Equation (17) can be rewritten as

$$\mathrm{SHF}_c = KA + B, \tag{20}$$

where $K$ was obtained by the least squares method. Using (17) with the derived coefficient $K$, we can calculate the time series of the sensible heat flux on the basis of the satellite data.

### b. Comparisons with NCEP and GSSTF sensible heat fluxes

We chose NCEP air temperature data during the period from July 1993 to December 1998 for computing the NCEP sensible heat flux and making a comparison with the calculated sensible heat flux. The NCEP dataset was downloaded from a Web site, which can be found online at http://www.cdc.noaa.gov/cgi-bin/nph-nc/Datasets/ncep.reanalysis.derived/surface/air.mon.mean.nc. Using NCEP air temperature data, the satellite sea surface temperature, and SSM/I wind speed, we calculated monthly time series of the sensible heat flux from July 1993 to December 1998, which is denoted as $\mathrm{SHF}_N$. In the other way, sensible heat flux was calculated on the basis of (17) and is represented as $\mathrm{SHF}_A$. To compare the two kinds of the sensible heat fluxes, we calculated root-mean-squares (rms) of the difference and correlation coefficient between $\mathrm{SHF}_A$ and $\mathrm{SHF}_N$, which are shown in Figs. 1a and 1b, respectively. The minimum rms is 10.0 W m$^{-2}$ and is located at 34°N, 151°E in the Kuroshio Extension area east of Japan. The region with the low rms is located between latitudes 33° and 36°N and between longitudes 143° and 156°E, which corresponds to the region with large atmospheric convergence over the test area (Pan et al. 2002). Figure 1b shows the correlation coefficient between NCEP and calculated sensible heat flux. One can see that low-rms region is consistent with that with high correlation coefficient ($>0.7$). In the test area, we define an atmospheric convergence zone where the long-term average of the atmospheric convergence is larger than $1.0 \times 10^{-6}$ s$^{-1}$, namely, the area $\Omega$, in which the following relationship is held:

$$-\overline{\left(\frac{\partial u}{\partial x} + \frac{\partial v}{\partial y}\right)} > 1.0 \times 10^{-6}. \tag{21}$$

We calculated the mean rms of the sensible heat flux difference between NCEP data and the calculations using (17) in the area $\Omega$, and it is 21.2 W m$^{-2}$.

Figure 2 shows comparisons between the two kinds of sensible heat fluxes from NCEP data and from the wind convergence at 10 locations in the sea area east of Japan. The latitudes and longitudes are listed in the figure panels. Asterisks represent the SHF from *ERS-1* winds and open circles denote that from *ERS-2*. The rms

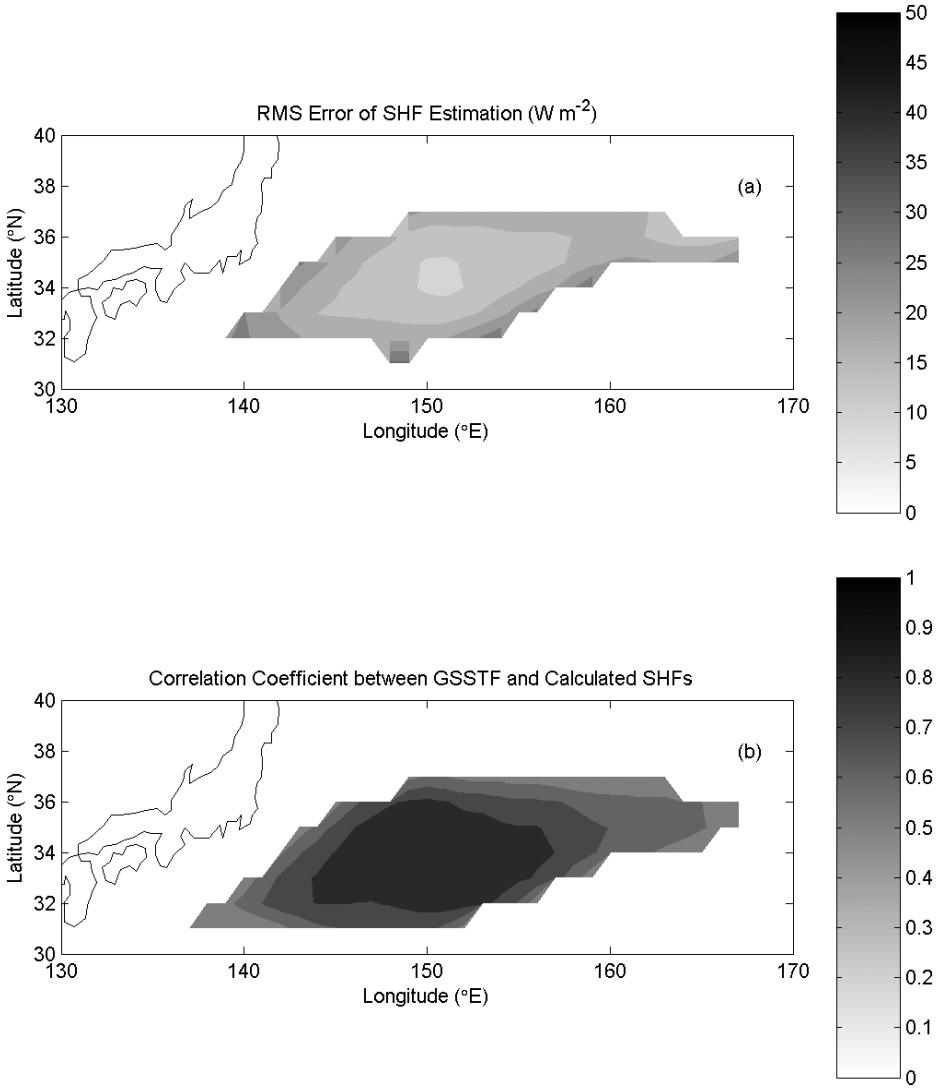


FIG. 4. (a) Rms difference and (b) correlation coefficient between the sensible heat flux calculated from satellite data and NASA GSSTF sensible heat flux.

of the sensible heat flux difference is in a range between 10.0 and 14.1 W $m^{-2}$. One can see that at these locations the two sensible heat fluxes are in agreement. However, in some years and at some locations, there are discrepancies. The figure shows that the calculated sensible heat fluxes have larger undulations year by year at these locations than the NCEP data. Among these locations, the time series of NCEP fluxes have less change than the calculated heat fluxes, which might result from model resolution limitations. Figure 3 illustrates the scatterplot of the two kinds of the sensible heat fluxes at the 10 locations. These scatter asterisks are distributed around the 1:1 line (the solid line in Fig. 3) within a limited range. In order to quantify the scatter of these scatter points off the 1:1 line, we defined a vertical distance between an asterisk and the 1:1 line and calculated the mean, which is 6.9 W $m^{-2}$.

To make a further comparison, we used another kind of the sensible heat flux, NASA Goddard Satellite-Based Surface Turbulent Flux (GSSTF), which is mainly based on SSM/I on board *F8*, *F10*, *F11*, *F13*, and *F14* satellites and was generated by Chou et al. (2001). The dataset can be found online at the NASA Web site: http://daac.gsfc.nasa.gov/CAMPAIGN_DOCS/hydrology/hd_gsstf2.0.html. The details of the data can be found in the GSSTF documents (Chou et al. 2001). As for the comparison between the GSSTF data and the calculated results, we obtained the rms of the sensible heat flux difference, which is shown in Fig. 4a. The minimum is found at 34°N, 151°E to be 12.2 W $m^{-2}$. The region with the low rms is located between 33° and 36°N and 143° and 156°E, same as that in the comparison between NCEP data and the calculated sensible heat flux. From Fig. 4b, showing the correlation coefficient between the

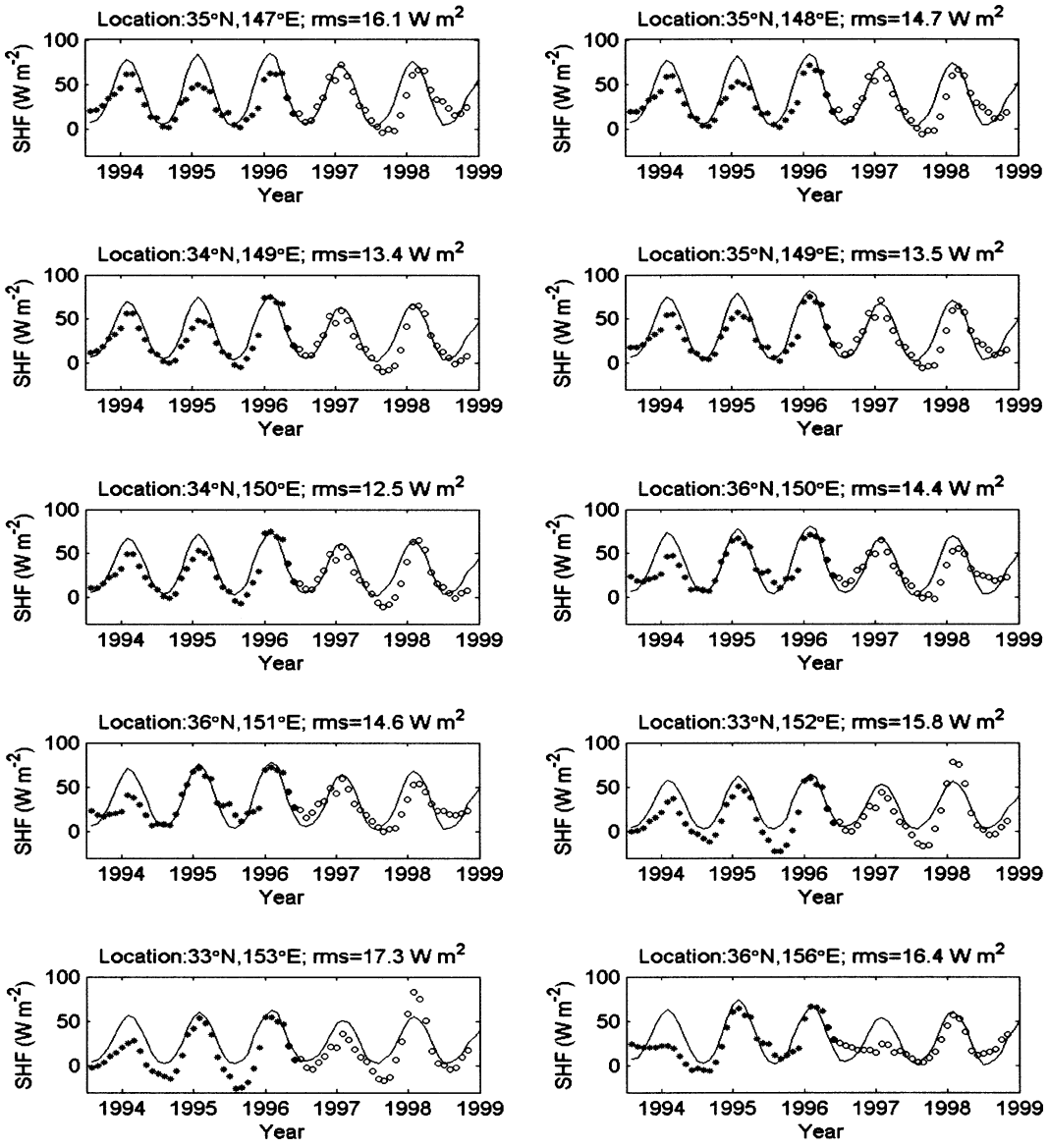


FIG. 5. The time series of satellite-data-calculated sensible heat flux (*: *ERS-1*, ○:*ERS-2*) and NASA GSSTF sensible heat flux (solid line) at 10 locations in the test area from Jul 1993 to Dec 1998.

GSSTF and computed sensible heat flux, one can see that the low-rms region corresponds to that with high correlation coefficient ($>0.7$). Over the previously defined atmospheric convergence zone, the mean rms of the difference is 22.5 W $m^{-2}$, slightly higher than the comparison with NCEP data. Figure 5 shows the time series of sensible heat flux at 10 locations in the atmospheric convergence zone. The rms is between 12.5 and 17.3 W $m^{-2}$. A scatterplot was generated and is shown in Fig. 6, which indicates the distribution of the sensible heat flux estimation with respect to the 1:1 line (shown as solid line in Fig. 6). Like the previous comparison, the mean distance between the asterisks and the 1:1 line is calculated as 8.5 W $m^{-2}$.

## 5. Discussions and conclusions

In this study, we developed a new method to estimate the sensible heat flux on the basis of the state equations using the wind convergence, sea level humidity, and sea surface temperature. The basic physical idea of the method is that atmospheric convergence may appear by the heating of the warmer sea surface water. The atmospheric convergence is related to the air–sea temperature difference, which is an important parameter for sensible heat flux estimation. We derived a theoretical formula, which related sensible heat flux to the atmospheric convergence. In the theoretical formula, Eq. (17), we determine the coefficient $K$ using the clima-

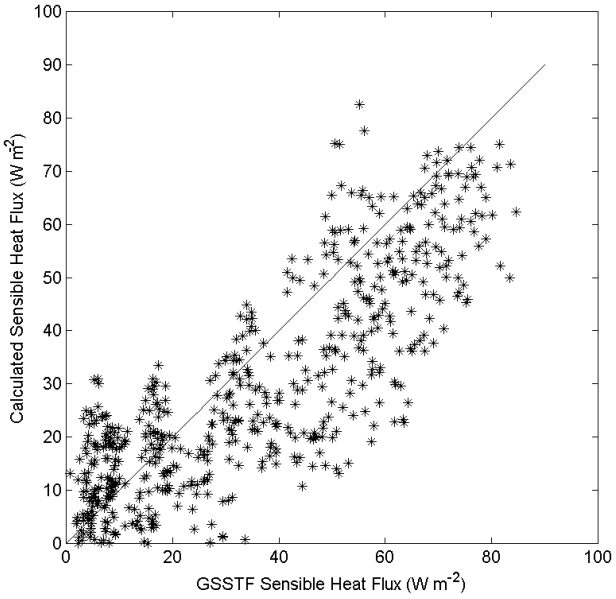


FIG. 6. Scatterplot of the satellite-data-calculated sensible heat flux and NASA GSSTF sensible heat flux at 10 locations in the test area.

tological data, assuming that $K$ changes only place to place, and ignoring temporal variations because of lacking knowledge of $K$. In (10), $K$ is defined as $dz/dt$, which has the velocity unit (m s$^{-1}$). Actually, $K$ does not only represent $dz/dt$. By Eq. (10), we have

$$\frac{\Delta\rho}{\rho}g = \frac{dw}{dz}\frac{dz}{dt},$$

where $dw/dz$ is calculated using $\Delta w/\Delta z$, and $\Delta w/\Delta z = -(\Delta u/\Delta x + \Delta v/\Delta y)$. Because $\Delta\rho$ only appears in the low level of the atmosphere, the scale of $z$ in $dz$ is smaller than in $\Delta z$. Therefore, we introduce a scale adjustment factor as $K_a$ in Eq. (10), and the right-hand side of (10) changes as

$$\frac{\Delta w}{\Delta z}\frac{dz}{dt}K_a,$$

and $K$ is adjusted as $(dz/dt)K_a$, which still has the velocity unit; $K$ is shown in Fig. 7. One can see that values are in the range between 65 and 150 m s$^{-1}$ in the test area.

To validate this method, we used two kinds of the sensible heat fluxes to make comparisons with the calculated flux. One is based on the NCEP air temperature and the other is the NASA GSSTF sensible heat flux. Comparison results show that the mean rms difference between the sensible heat fluxes from NCEP data and from satellite data is 21.2 W m$^{-2}$ for an atmospheric convergence zone in the test area east of Japan, and the correlation coefficient is greater than 0.7. The time series of sensible heat fluxes from NECP data and the analytical calculations at 10 locations in the area are in agreement, and the rms of the difference between the sensible heat fluxes ranges between 10.0 and 14.1 W m$^{-2}$. The comparison between the calculated heat flux and GSSTF heat flux reveals that the rms is 22.5 W m$^{-2}$ for the atmospheric convergence zone in the test area with the correlation coefficient greater than 0.7. The time series of the sensible heat fluxes at 10 locations in the test area are basically consistent, and the rms of sensible heat flux difference ranges between 12.5 and 17.3 W m$^{-2}$. Scatterplots suggest that the comparison with NCEP data gives better results. The calculated sensible heat flux is systematically less than the GSSTF data. This feature might result from the nonlinearity of the bulk formula, which results in a difference between the monthly mean of the sensible heat flux and that calculated from the monthly average of temperatures

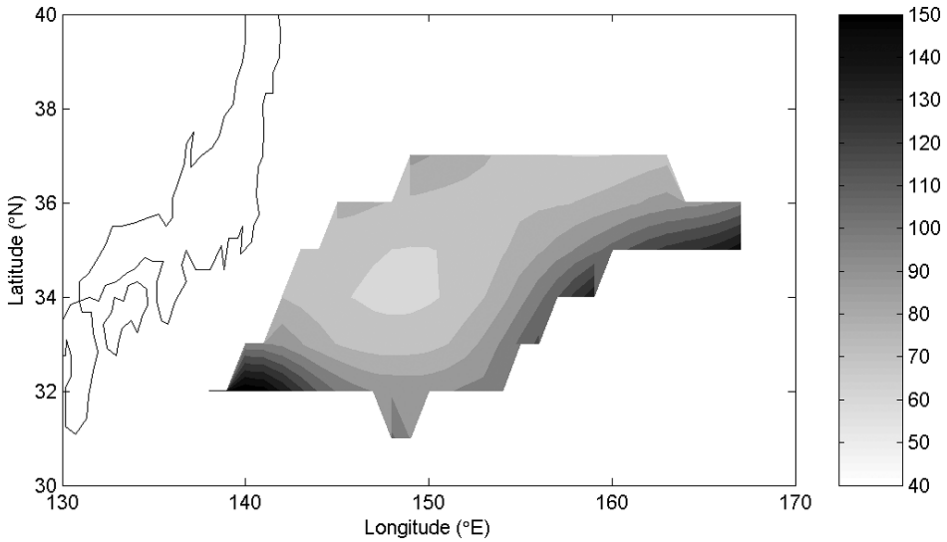


FIG. 7. The values of $K$ (m s$^{-1}$) in the test area east of Japan.

and winds. Considering this fact, we believe that the two comparisons are consistent with each other.

*Acknowledgments.* J. Pan and X.-H. Yan were supported by the National Aeronautics and Space Administration (NASA NAG5-11773) and the National Science Foundation (NSF OCE-9453499). W. T. Liu was supported by the NASA Ocean Vector Wind Science and Physical Oceanography Programs.

## REFERENCES

Bagno, A. V., and V. B. Zalesny, 1992: Numerical modeling of the North-Atlantic climatic thermohaline circulation. *Oceanologiya,* **32,** 789–800.

Baumgartner, M. F., and S. P. Anderson, 1999: Evaluation of regional numerical weather prediction model surface fields over the Middle Atlantic Bight. *J. Geophys. Res.,* **104,** 18 141–18 158.

Bigg, G. R., 1996: *The Oceans and Climate.* Cambridge University Press, 278 pp.

Cai, W., and S. J. Godfrey, 1995: Surface heat-flux parameterizations and the variability of thermohaline circulation. *J. Geophys. Res.,* **100C,** 10 679–10 692.

Chou, S.-H., E. J. Nelkin, J. Ardizzone, R. Atlas, and C.-L. Shie, cited 2001: Goddard Satellite-Based Surface Turbulent Fluxes (GSSTF)—Version 2: Documentation. [Available online at ftp://lake.nascom.nasa.gov/data/TRMM/Ancillary/gsstf/gsstf2.0/gsstf2_doc.]

Giese, B. S., and D. R. Cayan, 1993: Surface heat-flux parameterizations and tropical Pacific sea-surface temperature simulations. *J. Geophys. Res.,* **98C,** 6979–6989.

He, Y., X.-H. Yan, and W. T. Liu, 1997: Surface heat fluxes in the western equatorial Pacific Ocean estimated by bulk parameterization and by an inverse mixed layer model. *J. Phys. Oceanogr.,* **27,** 2477–2487.

Konda, M., N. Imasato, and A. Shibata, 1996: A new method to determine near-surface air temperature by using satellite data. *J. Geophys. Res.,* **101C,** 14 349–14 360.

Large, W. G., and S. Pond, 1982: Sensible and latent heat flux measurements over the ocean. *J. Phys. Oceanogr.,* **12,** 464–482.

Liu, W. T., 1986: Statistical relationship between monthly mean precipitable water and surface-level humidity over global oceans. *Mon. Wea. Rev.,* **114,** 1592–1602.

——, W. Tang, and F. J. Wentz, 1992: Precipitable water and surface humidity over global oceans from Special Sensor Microwave Imager and European Center for Medium-Range Weather Forecasts. *J. Geophys. Res.,* **97C,** 2251–2264.

Pan, J., X.-H. Yan, Q. Zheng, and W. T. Liu, 2002: Observation of western boundary current atmospheric convergence zones using scatterometer winds. *Geophys. Res. Lett.,* **29,** 1832–1835.

Simon, B., P. C. Joshi, and P. C. Pandey, and T. C. Panda, 1998: Air–sea flux estimates from satellite observations. *Indian J. Mar. Sci.,* **27,** 30–34.

Thadathil, P., A. Shikauchi, Y. Sugimori, and M. Kubota, 1993: A statistical method to get surface level air-temperature from satellite observations of precipitable water. *J. Oceanogr.,* **49,** 551–558.

Vazquez, J., A. V. Tran, R. Sumagaysay, E. Smith, and M. Hamilton, 1996: NOAA/NASA AVHRR Oceans Pathfinder sea surface temperature data set: User's guide. Jet Propulsion Laboratory, Pasadena, CA. [Available online at http://podaac.jpl.nasa.gov/pub/sea_surface_temperature/avhrr/pathfinder/doc/usr_gde1_3.html.]

Zheng, Q., X.-H. Yan, and W. T. Liu, 1997: Seasonal and interannual variability of atmospheric convergence zones in the tropical Pacific observed with ERS-1 scatterometer. *Geophys. Res. Lett.,* **24,** 261–263.